Environ Monit Assess (2018) 190:683
https://doi.org/10.1007/s10661-018-7070-z

A low-cost towed video camera system for underwater surveys: comparative performance with standard methodology

G. A. Trobbiani · A. Irigoyen · L. A. Venerus · P. M. Fiorda · A. M. Parma

Received: 24 June 2018 / Accepted: 22 October 2018

Abstract Technological advances in the field of underwater video have led to an exponential increase in the use of drifting cameras (DC) and remotely operated vehicles (ROVs) to monitor the diversity, abundance, and size structure of marine life. Main advantages of DCs relative to ROVs are their lower costs and the much simpler logistics required to operate them. This study compares the performance of a new low-cost DC system equipped with a novel measuring device with that of a standard DC bearing an array of laser pointers. The new DC, which can be operated from a small boat, carries a pair of parallel steel "whiskers" that are dragged on the seabed within the field of view of the camera, providing a scale for measuring and estimating the density of benthic biota. An experiment conducted using an array of objects of known sizes laid on the bottom showed that its performance in terms of both size and density estimation was similar to that of the standard technique based on laser pointers. Measurement errors had a negligible negative bias (−2.3%) and a standard deviation that ranged between 13 and 8% for objects from 25 to 110 mm in size. The whiskers offered a simplified method for density estimation that avoids the need to calculate the width of the field of view, thus reducing the video processing time by around 60% with respect to the standard method. Briefly, the new system offers an efficient low-cost alternative for benthic ecology studies conducted on soft or non-irregular bottoms.

Keywords Remote underwater video · Drifting camera system · Density estimation · Size measurement · Laser pointers

Electronic supplementary material The online version of this article (https://doi.org/10.1007/s10661-018-7070-z) contains supplementary material, which is available to authorized users.

G. A. Trobbiani (✉) · A. Irigoyen · L. A. Venerus · P. M. Fiorda · A. M. Parma
Centro para el Estudio de Sistemas Marinos (CESIMAR), Consejo Nacional de Investigaciones Científicas y Técnicas (CCT CONICET – CENPAT), Boulevard Brown 2915, (U9120ACD), Puerto Madryn, Chubut, Argentina
e-mail: gastontrobbiani@hotmail.com

Introduction

The use of underwater video to study marine life has gained wide acceptance in recent years (e.g., Mallet and Pelletier 2014; Whitmarsh et al. 2017). This is mainly because they overcome some of the drawbacks of more traditional removal sampling techniques such as trapping and trawling, which may be too costly (large fishing vessels are often needed), and limited by the roughness of the seabed or by fishing restrictions within marine protected areas. Remote video techniques allow collecting information about populations and communities in a non-destructive manner, while avoiding some of the limitations and biases of other non-intrusive methods such as underwater visual censuses (UVCs). They are free from depth and diving time constraints imposed by diving safety (Harvey and Shortis 1996; Harvey et al. 2001a, 2002), are not restricted by the presence of dangerous fauna (Meekan and Cappo 2004), and avoid biases caused by behavioral responses

Published online: 29 October 2018

of organisms to divers (Dickens et al. 2011). In addition, the video footage can be saved so that estimates can be replicated by different observers and images may be re-processed with new objectives. The main shortcomings of underwater video are the high equipment costs (although they are becoming more affordable), its limited application in turbid waters (which also limits the utility of UVC, but see Chidami et al. 2007 and Wilson et al. 2015), and time-consuming video processing (Shortis et al. 2009).

The use of underwater video also offers some advantages for estimating the size of objects compared to visual estimation by divers where precision depends on divers experience and is rarely measured (e.g., Harvey et al. 2002; Edgar et al. 2004). With video, objects can be measured accurately and unbiasedly and the magnitude of the measurement errors are regularly reported (Harvey et al. 2002; Spencer et al. 2005; Morrison and Carbines 2006; Cappo et al. 2007; Rooper 2008; Rosenkranz et al. 2008; Mallet and Pelletier 2014). Different techniques have been employed and their associated measurement errors depend on the technical features of the cameras and lenses, the design of the devices, and the optical characteristics of the seawater (Van Rooij and Videler 1996; Yoshihara 1997; Harvey et al. 2001b). The most common measuring techniques employ fixed-scale bars included in the camera field of view (Priede et al. 1994; Willis and Babcock 2000; Stobart et al. 2007), parallel laser-beam pointers (Love et al. 2000; Rochet et al. 2006; Rohner et al. 2011), and stereo-video (Harvey et al. 2002; Watson et al. 2005; Shortis et al. 2008). Among these, a difficulty with the incorporation of fixed-scale bars in the camera field of view is that the scale bar has to be in the same plane as the object being measured, something that rarely happens. Even subtle deviations from that requirement can produce large over- or under-estimation of size (Harvey et al. 2002; Stobart et al. 2007; Brooks et al. 2011; Trobbiani and Venerus 2015). For systems bearing lasers, a minimum of two laser spots projected on the object to be measured (or close to it) provides a reference scale within the images (e.g., Pilgrim et al. 2000; Deakos 2010; Rohner et al. 2015). When the laser beams are reflected by the object or by a surface located approximately in the same plane, perpendicular to the laser beams, the size estimation is independent of the focal distance. Here too sizes will be over- or under-estimated when the objects are, respectively, closer to or further from the camera than the reference provided by the laser spots. Although the use of laser is simple and inexpensive, the probability of impacting an object with the correct beam angle may be extremely low if the lasers are attached to immobile or uncontrolled devices (Gledhill et al. 2005). In stereo-video systems, two cameras separated by a fixed distance converge towards the point at which both focal lines cross. These more sophisticated systems can reduce measurement errors at the expense of increasing equipment and software costs, although a few free and low-cost options are now available (Bouguet 2008; Delacy et al. 2017).

A new video remote drifting camera system called "PEPE" was developed by Trobbiani and Irigoyen (2016) as a simple, low-cost alternative to standard laser-based techniques for estimating size and density of fishes and invertebrates lying close to the seabed. It consists of a DC that hauls two long steel cables —"whiskers"—which provide a fixed width reference within the camera field of view used to estimate the swept area and the size of any object lying on the sea bottom. The aim of this study is to compare the performance of this new system with that of a classic DC bearing an array of laser pointers, in terms of ease of use, processing time, and accuracy and precision of the measurements obtained. We also discuss how to synchronize the time between GPS and the video for geolocalizing the target fauna with the DC cameras.

Materials and methods

Drifting camera configuration

We constructed two DC systems, one carrying a pair of steel whiskers (PEPE) and the other bearing an arrangement of laser pointers (called RAFA) (Fig. 1). In both cases, the towed structure holds two cameras: one vertical, pointing to the seabed (*slave*) used for estimating the sizes and densities of animals and plants lying or attached to the seabed, and the other horizontal, pointing forward in the direction of the drag (*exploratory*; see Fig. 1) used to control the DC height from bottom and to avoid potential collisions with any artificial structure or rocky outcrops. The exploratory camera is connected to a 14-in. color monitor installed onboard the boat through a class-5 FTP (foiled twisted pair), with overall screen and

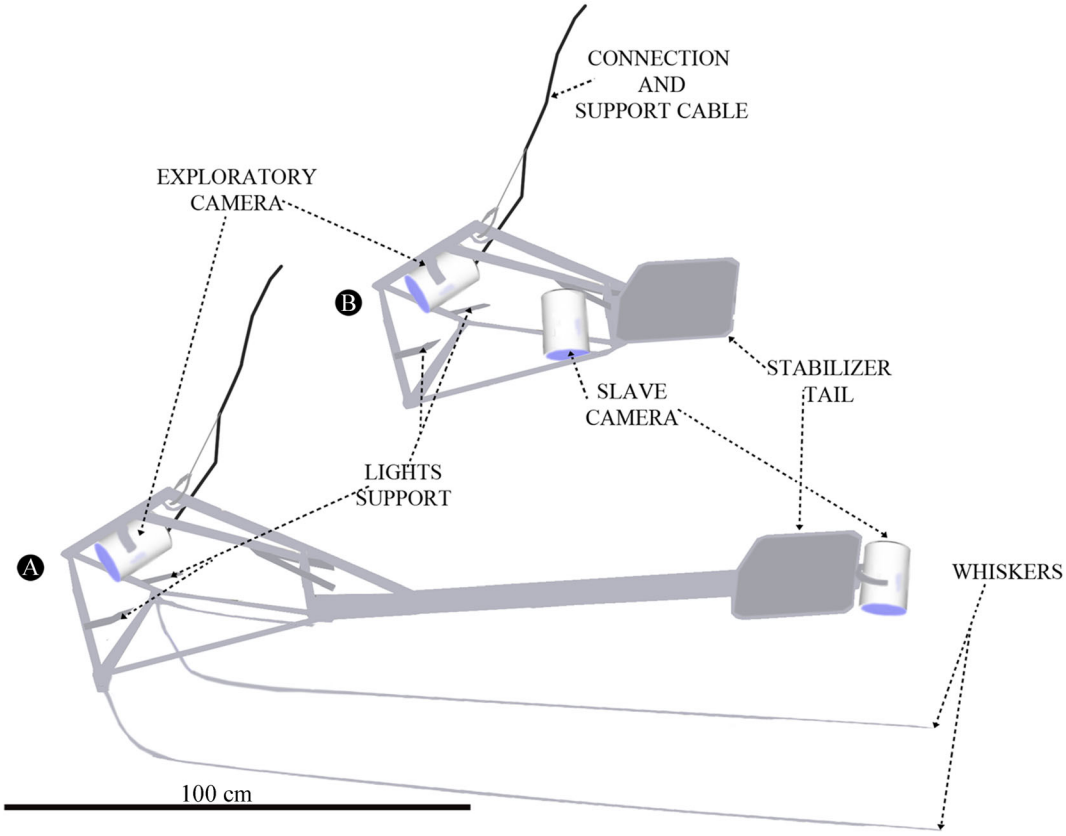

Fig. 1 Diagrams of the two systems of drifting cameras (DC) compared in this study. **a** PEPE, developed by Trobbiani and Irigoyen (2016). **b** RAFA, a classic DC. From left to right: exploratory camera, support for lights, support and connection cables, slave camera, stabilizer tail, and whiskers (only in **a**)

supporting steel wire. The slave camera is located on the back but it is not connected to the surface. Both cameras are housed in plastic matrixes inside home-built waterproof compartments, resistant up to 15 atm. These compartments are entirely made of stainless steel with a 20-mm-thick acrylic lid. The video-cameras (see below) were controlled (on/off and recording/stop) at the surface, before deploying them, using a remote control via Wi-Fi connection. The Wi-Fi connection facilitated the development of watertight compartments with reduced costs and complexity (i.e., no turn on/off buttons were necessary).

As described by Trobbiani and Irigoyen (2016), PEPE's frame is 177 cm long × 30 cm wide × 28 cm tall and has two whiskers attached to the front (Fig. 1a), consisting of two parallel 4-m-long steel cables, separated by 50 cm. As the distance between the cables remains constant while they are towed in contact with the bottom, the whiskers provide a fixed scale in the video footage of the slave camera (Fig. 2a).

RAFA (Fig. 1b) has an array of five parallel laser pointers embedded in the same plastic matrix that houses the slave camera. The laser beams point to the seabed and add a fixed scale that is captured by the slave camera (Fig. 2b).

GoPro video cameras (Hero 3 and 3+ silver edition models) were used for the experiment. Video resolution was selected at 1080p = 1920 × 1080 pixels (16:9).

Study site, experimental design, and data collection

An experiment aimed to compare the performance of PEPE DC with that of a classic DC bearing an arrangement of laser pointers was carried out in Nuevo Gulf, Argentina (42.77°S, 65.00°W) in October 2014. An array of 200 plastic pipe sections of different known sizes, emulating sessile animals, was set up on the bottom and later surveyed using the two DC devices to evaluate errors made in the estimation of sizes and density. The seafloor in this area consists of consolidated clay with

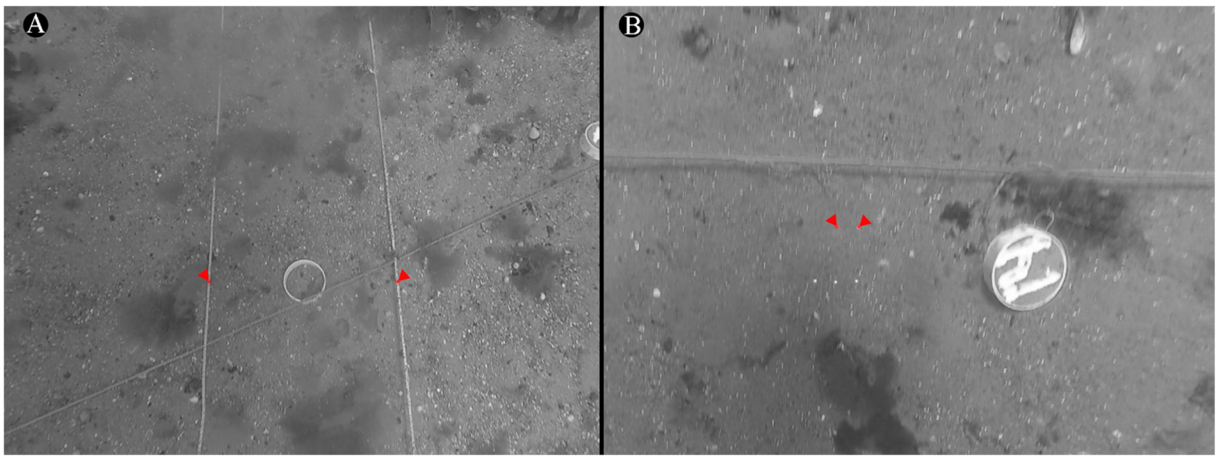

Fig. 2 Video frames captures from the DC systems showing a detail of the measuring scales. **a** PEPE's steel cables captured by the slave camera, separated by 50 cm. **b** RAFA's array of five parallel laser pointers separated horizontally by 3 cm. Only the upper two are marked with red triangles

scattered patches of seaweed and the depth ranged between 6 and 10 m (depending on the tidal level).

Four parallel lines of 50-m length, with 50 pipe sections of a given size attached to them, were laid on the seabed, separated 4 m from each other, covering a rectangular grid of 50 m × 12 m. The grid was marked at the surface by four buoys attached to the bottom by iron stakes. The plastic pipes were 25, 40, 63, and 110 mm in diameter (50 of each size) and 30 mm in height. These sizes were chosen so as to cover the size range of the most common epibenthic macrofaunal organisms in the region (Roux et al. 1995). Pipe sections were tied to the lines and fixed with small iron stakes to the bottom, to ensure that the transversal circular sections pointed to the sea surface. Half of the pipe sections of 110 mm ($n = 25$) were filled with cement, numbered, and georeferenced by a diver.

Video-transects were obtained with both DCs, which were slowly towed (three knots maximum speed) from a 4.5-m pneumatic boat. The two DC systems are light (less than 12 kg) and were manually operated. Two operators are required, one to deploy the equipment and the other to control the distance of the camera from the bottom (manually), and to record all necessary data (position, speed, and video timer). The DCs were hauled from 0.5 to 1 m above the seabed, perpendicularly to the lines. The RAFA DC was trawled closer to the sea bottom (~0.5 m) than PEPE, so that the laser points could be clearly seen. A total of 15 video-transects were recorded with PEPE and 11 with RAFA while tracking the boat trajectories with a GPS.

Data processing and analysis

Video footages were played on a computer and the snapshots containing pipe sections were extracted with the software Sony Vegas (SVS; see details in Online Resource I) which allows the user to save the time of occurrence of events using hotkeys. An event in our case was defined as the presence of a pipe section located approximately in the middle of the vertical field of view of the camera (Fig. 2). Each snapshot may contain more than one pipe section. The time of each event in the video footage was saved into a list, which was used to extract the snapshots automatically with the *avconv* tool (http://libav.org), using an ad hoc script written in *bash* language (Online Resource II). A total of 55 images were extracted from PEPE's video footage and 37 from RAFA's. The snapshots were used to estimate the size of the objects and the width of the camera field of view, which was in turn used to estimate the total swept area per transect. Data are available upon request to the authors.

Georeferencing

The GPS tracks were synchronized with their corresponding video footage in order to approximate the position of the objects recorded in the video from the boat's position. The errors made in this approximation were calculated by estimating the actual position of 11 numbered pipe sections observed in PEPE's

video. To do that, a diver positioned himself on the surface right above each of the marked pipes, with the aid of a plumb and a rope, and marked a waypoint with a GPS (Garmin, model *Extreme Legend*). These positions were considered accurate aside from GPS errors. The list of event-times recorded while processing the videos was used to locate each numbered pipe section on the GPS track, and the distance between this location and the actual position registered by the diver was calculated using the vectorial tools of the Qgis software v.2.18.0.

Density estimation

All pipe sections identified in each video transect were counted and used to estimate the average density per transect and the total numbers in the experimental plot. Counts were made with the (SVS), which allows varying playback speed. The saved snapshots were used to estimate the total area swept along each transect made with both DCs. First, the width of the field of view recorded in each snapshot ($n = 59$ for PEPE and $n = 41$ for RAFA) was calculated from the scales of known size (whiskers or laser points, respectively), and an average width (AW) was estimated for each transect. Second, the length of each transect ($n = 15$ for PEPE and $n = 11$ for RAFA) was obtained from their GPS tracks and assumed known without error. An area-weighted average density of pipe sections was estimated by dividing the total counts by the total swept area over all transects. The standard error and 95% confidence intervals for the average density for each method were estimated by a nonparametric bootstrap on transects ($n =$ 50,000).

In addition, a simpler alternative procedure for estimating density was tried with PEPE consisting of counting only those pipe sections located between the whiskers, and estimating the transect area as the product of the transect length (GPS track data) and the distance between whiskers (50 cm), hereafter referred to as PEPE WA. Although this method uses a much smaller sampling area (approximately one third of the total field of view of the cameras), its main advantage is that the area estimation is fast and straightforward.

Resulting estimates of the total number of pipe sections in the experimental plot were compared to the known number of objects (=200) to evaluate the relative errors of the different techniques.

Size estimation

Three operators measured the diameters of the pipe sections using the same set of images. The free software *ImageJ* was used to scale the images with the fixed reference scale included in the image (50 cm between the whiskers in PEPE's images and 3 cm between the laser spots in RAFA's; Fig. 2). All the pipe sections located within the field of view were measured in both cases. A few snapshots were discarded because pipe sections were tilted and could not be measured reliably. Measurements were directly stored in a text file for later analysis without the operator knowing the value of the measurement taken.

To evaluate the performance of the prototypes and to quantify the bias and dispersion of size estimates, we used linear mixed-effect and generalized least squares (i.e., gls) models implemented in the package "*nlme*" v.3.1–136 (Pinheiro and Bates 2000) of the R software (R Development Core Team 2015). The relative measurement error (dependent variable) was modeled as a function of two factors: the DC prototype (two levels: PEPE and RAFA) and the true size of the measured objects (four levels: 25 mm, 40 mm, 63 mm, and 110 mm). These factors, as well as their interactions, were tested as fixed factors while the identity of the operator measuring the sections (three different operators) was included as a random effect. The initial examination of the data suggested heterogeneous variances; therefore, we evaluated different variance functions: variance as a linear (varFixed) or power (varPower) function of the object size with coefficients that could differ between DC systems, a different variance for each of the different combinations of the factors "DC" and "diameter" (varIdent), and a combination of varIdent and varPower, where both the factor and the power coefficient could differ between DC systems. The fixed terms of the models were tested by fitting the models using maximum likelihood (ML) while the random terms and variance functions were evaluated using the restricted maximum likelihood (REML) method (Zuur et al. 2009). We used the Akaike's information criterion (AIC) for model selection (Burnham and Anderson 2002).

Video processing time

We recorded the time required to analyze the videos in the laboratory, including the processes of counting and

measuring the objects, and the scaling of the snapshots to estimate the swept area. The extraction of images from the videos for later analysis was done automatically for both DCs. The time associated with the setting up of the equipment and with the calibration of the whiskers and laser pointers was not included in this analysis.

Results

A total of 15 transects was completed with the PEPE DC and 11 with RAFA, taking 18 min and 16 min, respectively, over a single video recording session with each DC system.

Georeferencing

The distances between the actual position of the pipe sections (estimated by the diver) and the position estimated from boat track ranged between 0.81 and 10.1 m (mean = 4.79 m; SD = 2.36). This mean value was within the error of the GPS used (1 to 5 m).

Density estimation

The mean transects' width was 2.06 m (± 0.65 m) for PEPE and 1.12 m (± 0.27) for RAFA. Transect lengths ranged from 8 to 14 m for PEPE, and from 12 to 14 m for RAFA, resulting in respective mean swept areas per transect of 26.33 m^2 (± 2.18 m^2) and 14.52 m^2 (± 3.6 m^2). For the simplified density estimation method, the width was constant and the total mean between whisker area per transect was 6.3 m^2 (± 0.8m^2). Mean densities estimated by the three methods did not differ and were close to the true density of pipe sections in the experimental plot (0.310 pipe sections/m^2; Table 1).

Size estimation

Preliminary data exploration showed a tendency to underestimate size with the two DC systems. Median relative errors for the different size classes ranged between − 0.045 and − 0.009 for PEPE, and between − 0.045 and 0.001 for RAFA (Fig. 3a). When all pipe sections were pooled, the median relative error was − 0.019 and − 0.032 for PEPE and RAFA, respectively. The estimates obtained with PEPE were more dispersed (Fig. 3b). There were no obvious differences between operators (Fig. 3c).

The comparison of the full mixed-effect model (including all explanatory variables) with one that did not include random effects (except for the residuals) indicated that the variance contributed by the operator was not significant. Therefore, the subsequent models were all fitted using *gls*. None of the fixed effects tested improved the model fit significantly, as evaluated by the AIC assuming a different variance coefficient for each combination of DC and object diameter (the most flexible variance function evaluated). Hence, the fitted *gls* had a single fixed term representing the overall bias (− 0.023) in the size measurements for the two DC systems.

In terms of the variance structure, we selected two *gls* models with very similar AIC (Table 2), in which the variance of the relative measurement error decreased as a power function of the object size. In the first model, the power coefficient differed slightly between the two DC systems, while in the second, the power coefficient was the same but the proportionality coefficient differed between the two DC systems. In both cases, the predicted standard deviation decreased sharply up to ca. 50 mm, and stabilized from there on. Over the range of sizes tested (25 mm to 110 mm), both models

Table 1 Average density of pipe sections (PS) and its standard error and 95% confidence intervals estimated by nonparametric bootstrap from video transects recorded with the two DC systems (PEPE and RAFA)

	Mean (PS/m^2)	SE	95% confidence Intervals		Number of pipe sections counted per transect (min-max)
			Lower	Upper	
RAFA	0.305	0.019	0.263	0.339	2–8
PEPE WA	0.355	0.043	0.266	0.437	1–4
PEPE	0.321	0.019	0.261	0.340	5–12

"PEPE WA" corresponds to the estimate based only on the objects counted within the area delimited by the whiskers. Pipe section density in the experimental plot = 0.310 PS/m^2

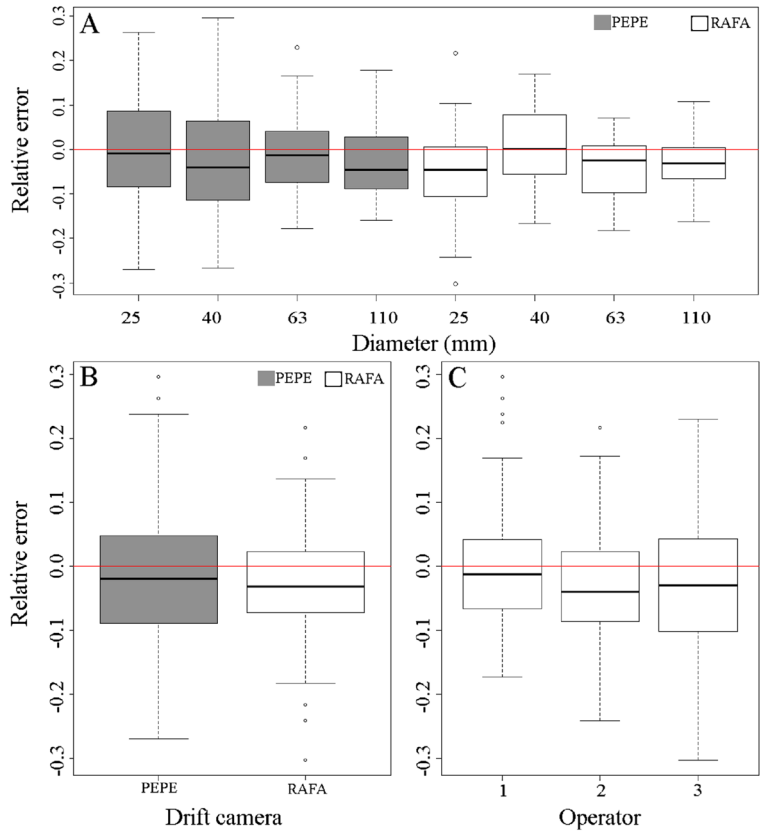

Fig. 3 Boxplots of **a** relative errors in size measurements for different pipe section diameters and drifting camera (DC) systems, **b** overall relative errors for the two DCs, and **c** overall relative for the three operators, pooling data for the two DCs

predicted a decrease from 0.13 to 0.08 for PEPE and from 0.10 to 0.06 for RAFA (Fig. 4).

Processing time

The processing time required for estimating density involved the total video-replay time for counting the objects—28 min for PEPE and 16 min for RAFA played in real time—plus some additional time used to extract and scale the snapshots (55 snapshots for PEPE and 37 for RAFA) in order to estimate transect width: 43 min for PEPE and 38 min for RAFA. No additional time was needed to estimate density using the simplified method based on PEPE's footage as the distance between the whiskers was considered known and constant (see Fig. 2a). In summary, the total processing time per transect

Table 2 Summary of the two selected *gls* models fitted to the relative errors of size estimates obtained using two drifting camera systems (PEPE and RAFA, see the text for details)

ID	Model	Parameters values (95% CI)	Model selection	
			df	ΔAIC
Model a	Relative error = intercept + ε_i; $\varepsilon_i \sim N(0, \sigma_i^2)$; $\sigma_i = a\lvert\text{diam}\rvert^{b_i}$; $i = 1,2$	Intercept = − 0.023 (− 0.033; − 0.013), a = 0.367 (0.206; 0.656), b_1 = − 0.324 (− 0.472; − 0.177), b_2 = − 0.387 (− 0.538; − 0.236)	4	0
Model b	Relative error = intercept + ε_i; $\varepsilon_i \sim N(0, \sigma_i^2)$; $\sigma_i = c_i\lvert\text{diam}\rvert^{d}$; $i = 1,2$	Intercept = − 0.023 (− 0.033; − 0.013), c_1 = 0.407 (0.225; 0.734), c_2 = 0.320 (0.179; 0.570), d = − 0.350 (− 0.498; − 0.202)	4	0.3

The components of the variance function for each model, parameter values, and the difference in AIC between the selected models are shown

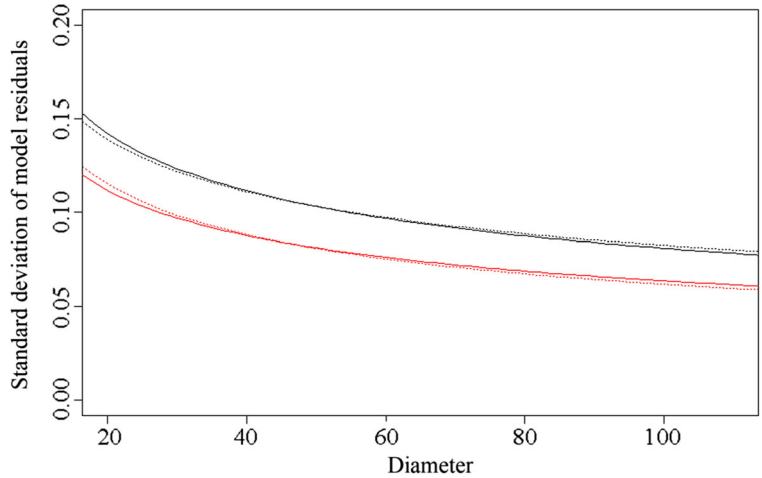

Fig. 4 Standard deviation of the relative measurement errors estimated with the two *gls* models selected. Line colors indicate the DC systems (PEPE: black lines, RAFA: red lines) and line types, the fitted models (model a: continuous lines, model b: dotted lines)

required for density estimation was 4.73 min for PEPE, 4.90 min for RAFA, and 1.86 min for PEPE WA. Thus, the simplified method required less than 40% of the processing time required by the other methods.

Measuring the objects (66 pipe sections in PEPE's footage and 42 in RAFA's) took an average of 1.05 min per pipe section for PEPE and 1.23 min for RAFA. Accounting for the total time required to scale the snapshots (used for density estimation) and to measure the pipe sections, it took 1.70 min per pipe section using PEPE's snapshots and 2.14 min per pipe section using RAFA's.

Discussion

In this paper we compared the performance of a newly designed DC that hauls a pair of steel whiskers serving as a reference scale introduced in the images, with standard measuring equipment bearing laser pointers. Our results indicate that the new equipment (PEPE DC) is an efficient, accurate, and cost-effective device, useful to estimate the density and size of sessile or less mobile aquatic organisms lying close to the sea bottom. There were no differences either in the size or in the density estimates obtained using the PEPE DC and a traditional laser-bearing DC (RAFA). Processing the videos, however, took considerably less time when using the novel method based on the steel whiskers (PEPE WA).

Both DC systems, PEPE (including a simplified estimate of the swept area, PEPE WA) and RAFA, produced similar density estimates that did not differ from the overall true density of pipe sections in the experimental plot. As is the case of other video systems described in the literature (e.g., Rooper and Zimmermann 2007; Tran 2013), the estimation of the swept area with PEPE and RAFA DCs requires calculating the width of each snapshot used to count the number of objects present. In the case of PEPE WA, the width of the video transect is given directly by the distance between the two parallel cables, considered constant. This simplified procedure for estimating the swept area reduced the video processing time by 60% at the expense of a reduction in the area used to estimate density, which in turn may affect the precision of the estimates. It is important to note that the choice of transects width in any visual census should be determined according to the density, distribution, and behavior of the target species (e.g., Cheal and Thompson 1997; Samoilys and Carlos 2000; Irigoyen et al. 2018).

Imperfect detectability, i.e., the inability to detect all individuals in a survey area (Katsanevakis et al. 2012), is one potentially important source of error that should be controlled in real applications. In our experimental conditions, detectability was not an issue given the high color contrast between the pipe sections (white) and the bottom (dark brown), the simple, flat bottom, and the high water visibility. The detection probability may decrease under low-light and turbid-water conditions, when the bottom is complex or when cryptic fauna is to be assessed. In turbid and low-light environments, reducing the towing speed or the distance between the DC and the bottom could contribute to increase detectability by improving the quality of the snapshots that could be retrieved from the videos.

The models fitted to the relative measurement errors obtained with the two DC systems compared indicated that both had a small tendency to underestimate the size of the objects (a bias of − 2.3%). The coefficient of variation (CV) of the measurements decreased with the size of the measured objects; this may be due to an inherent error in the delimitation of the objects contours, which depends on the image's pixel size and is constant on average, independent of object size (Harvey et al. 2001a). Because the DC system using lasers (RAFA) was towed closer to the bottom, its camera field of view was narrower resulting in a pixel size that was about 46% smaller on average than the pixel size in PEPE's snapshots. This difference may contribute to the smaller measurement error made using laser pointers (Fig. 4).

The size range of the objects used in this study (25 mm to 110 mm) comprises a wide spectrum of sessile and mobile benthic fauna. The usual problem inherent to the use of a single camera for measuring objects, where the object and the scale used to measure it must be at the same focal distance, did not represent a major inconvenience in this work as both the scale and the objects were on the bottom. On the other hand, trying to estimate the size of objects that are above the reference (whiskers/background) with this method would result in errors as reported by Trobbiani and Venerus (2015). The errors in size estimation obtained in this work (CV = 6–8% for objects of 110 mm in size) are in the order of those reported in the literature for other devices designed with similar purposes. Errors reported by Rochet et al. (2006) for objects of true size between 130 and 660 mm, resulting from the use of laser pointers as fixed scales, were in the range of 7 to 13% CVs for visual size estimations performed directly on the screen without using any measuring instrument, and between 1 and 4% for measurements taken after the acquisition and processing of the videos (as we did here). Our measurements were less accurate than those obtained by Harvey et al. (2002), who reported CVs of 1% when measuring 480-mm-long fish silhouettes using fixed scales included in the camera field of view and computer processing, and by Delacy et al. (2017), who reported errors <1% and < 3% in comparison with tape-measured lengths of sharks > 1 m in the pool and in the field, respectively. However, in a different study conducted using stereo video, Harvey and Shortis (1996) obtained CVs between 0.6 and 7.5% for fish silhouettes ranging in size from 100 to 470 mm.

For a comparable accuracy of measurements, the simplicity of the newly developed DC system (PEPE) offers some advantages relative to the standard use of lasers. The whiskers do not need any type of maintenance or calibration, and as they have no electrical or electronic components, in contrast to the use of laser pointers or stereo-video, they are not susceptible to fail at sea. The whiskers are also inexpensive and easy to replace quickly in the field. An important shortcoming of the whiskers method is that their use is restricted to rather flat bottoms, as the parallelism and constant distance between the two cables could be compromised when towed over irregular bottoms. Complex habitats, however, pose problems for underwater video in general as cryptic species may find refuge, and hence go unnoticed by the camera.

A wider use of this type of equipment and the possibility of the geolocation of video images would allow collecting information for habitat and macrobenthos mapping at low cost (for example, Raymond et al. 2008; Tran 2013). The accuracy of geolocation of a drifting systems, often requiring correction methods, depends on the depth and speed at which the equipment is towed, the water currents, the diameter of the cable with which it is held, and the weight of the equipment itself (Schories and Niedzwiedz 2012). These variables must be taken into account when making position corrections for the equipment relative to the boat. Alternatively, more complex and expensive systems (USBL, ultra-short baseline) for locating the DC underwater such as those used in Holmes et al. (2008) are available but they tend to be unaffordable in low-budget situations. In our experiment, similarly to other studies (e.g., Jordan et al. 2005; Tran 2013), the distance between the DC and the boat was small, in the order of the magnitude of the error reported for the GPS used. This reflected our particular experimental conditions: shallow waters, lack of currents, and low towing speed. Data taken at greater depths may require corrections of the position of the DC with respect to the boat (e.g., Hewitt et al. 2004).

Conclusion

Beyond the aforementioned advantages of the PEPE DC, this device is particularly useful in coastal areas. We have successfully used it up to 60-m depth in turbid water (visibility between 1 and 3 m), with strong

currents. The system is robust enough to be deployed from small boats by hand, and requires minimum personnel and training. The simultaneous use of an echo sounder during dragging is encouraged to prevent collisions with rocky outcrops. Future field tests on different aquatic environments with different purposes should be conducted to include, for example, the assessment of mobile demersal species, like highly mobile crabs or fishes, which were mostly captured by the exploratory camera but not by the slave camera.

Acknowledgements We would like to thank M. Funes, D. Galván, F. Irigoyen, N. Ortíz, N. Sánchez-Carnero, and the staff of the Administración de Parque Nacionales in Camarones for their help during fieldwork; MaxSea Naval S.L. provided the navigation tools.

Funding Financial support was provided by Youth Activity Fund (The Explorers Club, granted to GAT), Agencia Nacional de Promoción Científica y Tecnológica PICT 2012-0297 (granted to AMP), and Secretaría de Ciencia, Tecnología e Innovación Productiva del Chubut, Argentina (granted to GAT).

References

Bouguet, J. Y. (2008). *Camera calibration toolbox for MATLAB*. Available from: http://vision.caltech.edu/bouguetj/calib_doc/index.html (Jan. 2014).

Brooks, E. J., Sloman, K. A., Sims, D. W., & Danylchuk, A. J. (2011). Validating the use of baited remote underwater video surveys for assessing the diversity, distribution and abundance of sharks in the Bahamas. *Endangered Species Research, 13*, 231–243. https://doi.org/10.3354/esr00331.

Burnham, K. P., & Anderson, D. R. (2002). *Model selection and inference*. New York: Springer-Verlag 512p.

Cappo, M., Harvey, E., & Shortis, M. (2007). Counting and measuring fish with baited video techniques—an overview. In: D. Furlani, & Beumer J. P. (eds.) *Proceedings of the Australian Society for Fish Biology workshop, Hobart* (pp. 101–114).

Cheal, A. J., & Thompson, A. A. (1997). Comparing visual counts of coral reef fish: Implications of transect width and species selection. *Marine Ecology Progress Series, 158*, 241–248. https://doi.org/10.3354/meps158241.

Chidami, S., Guénard, G., & Amyot, M. (2007). Underwater infrared video system for behavioral studies in lakes. *Limnology and Oceanography: Methods, 5*, 371–378. https://doi.org/10.4319/lom.2007.5.371.

Deakos, M. (2010). Paired-laser photogrammetry as a simple and accurate system for measuring the body size of free-ranging manta rays *Manta alfredi*. *Aquatic Biology, 10*, 1–10. https://doi.org/10.3354/ab00258.

Delacy, C., Olsen, A., Howey, L., Chapman, D., Brooks, E., & Bond, M. (2017). Affordable and accurate stereo-video system for measuring dimensions underwater: A case study using oceanic whitetip sharks *Carcharhinus longimanus*. *Marine Ecology Progress Series, 574*, 75–84.

Dickens, L. C., Goatley, C. H. R., Tanner, J. K., & Bellwood, D. R. (2011). Quantifying relative diver effects in underwater visual censuses. *PLoS One, 6*, 6e18965. https://doi.org/10.1371/journal.pone.0018965.

Edgar, G. J., Barrett, N. S., & Morton, A. J. (2004). Biases associated with the use of underwater visual census techniques to quantify the density and size-structure of fish populations. *Journal of Experimental Marine Biology and Ecology, 308*, 269–290. https://doi.org/10.1016/j.jembe.2004.03.004.

Gledhill, C. T., Ingram, G. W., Rademacher, K. R., Felts, P., & Trigg, B. (2005). SEDAR10-DW12 NOAA Fisheries Reef Fish Video Surveys: Yearly indices of abundance for Gag (*Mycteroperca microlepis*). *SEDAR SouthEast Data, Assessment, and Review*. Gulf of Mexico Gag Grouper Stock Assessment Report. Section 2, Vol. 29414, 28 p.

Harvey, E. S., & Shortis, M. R. (1996). A system for stereo-video measurement of subtidal organisms. *Marine Technology Society Journal, 29*, 10–22.

Harvey, E. S., Fletcher, D., & Shortis, M. R. (2001a). A comparison of the precision and accuracy of estimates of reef-fish lengths determined visually by divers with estimates produced by a stereo-video system. *Fishery Bulletin, 99*, 63–71.

Harvey, E. S., Fletcher, D., & Shortis, M. R. (2001b). Improving the statistical power of length estimates of reef fish: A comparison of estimates determined visually by divers with estimates produced by a stereo-video system. *Fishery Bulletin, 99*, 72–80.

Harvey, E. S., Shortis, M. R., Stadler, M., & Cappo, M. (2002). A comparison of the accuracy and precision of measurements from single and stereo-video systems. *Marine Technology Society Journal, 36*, 38–49. https://doi.org/10.4031/002533202787914106.

Hewitt, J. E., Thrush, S. E., Legendre, P., Funnell, G. A., Ellis, J., & Morrison, M. (2004). Mapping of marine soft-sediment communities: Integrated sampling for ecological interpretation. *Ecological Applications, 14*, 1203–1216. https://doi.org/10.1890/03-5177.

Holmes, K. W., Van Niel, K. P., Radford, B., Kendrick, G. A., & Grove, S. L. (2008). Modelling distribution of marine benthos from hydroacoustics and underwater video. *Continental Shelf Research, 28*, 1800–1810. https://doi.org/10.1016/j.csr.2008.04.016.

Irigoyen, A. J., Rojo, I., Caló, A., Trobbiani, G. A., Sánchez-Carnero, N., & García-Charton, J. A. (2018). The "Traked roaming transect" and distance sampling methods increase the efficiency of underwater visual censuses. *PLoS One, 13*, e0190990. https://doi.org/10.1371/journal.pone.0190990.

Jordan, A., Lawler, M., Halley, V., & Barrett, N. (2005). Seabed habitat mapping in the Kent Group of islands and its role in marine protected area planning. *Aquatic Conservation – Marine and Freshwater Ecosystems, 15*, 51–70. https://doi.org/10.1002/aqc.657.

Katsanevakis, S., Weber, A., Pipitone, C., Leopold, M., Cronin, M., Scheidat, M. T., Doyle, T. K., Buhl-Nortensen, L., Buhl-Mortensen, P., D'Anna, G., De Boois, I., Dalpadado, P., Damalas, D., Fiorentino, F., Garofalo, G., Giacalone, V. M., Hawley, K. L., Issaris, Y., Jansen, J., Knight, C. M., Knittweis, L., Kröncke, I., Mirto, S., Muxika, I., Reiss, H.,

Skjoldal, H. R., & Vöge, S. (2012). Monitoring marine populations and communities: Methods dealing with imperfect detectability. *Aquatic Biology, 16*, 31–52. https://doi.org/10.3354/ab00426.

Love, M., Caselle, J., & Snook, L. (2000). Fish assemblages around seven oil platforms in the Santa Barbara Channel area. *Fishery Bulletin, 98*, 98–117.

Mallet, D., & Pelletier, D. (2014). Underwater video techniques for observing coastal marine biodiversity: A review of sixty years of publications (1952–2012). *Fisheries Research, 154*, 44–62. https://doi.org/10.1016/j.fishres.2014.01.019.

Meekan, M., & Cappo, M. (2004) Non-destructive techniques for rapid assessment of shark abundance in northern Australia. In *Produced for Australian Government Department of Agriculture, Fisheries and Forestry*. Townsville, AUS: Australian Institute of Marine Science. 29 p.

Morrison, M., & Carbines, G. (2006). Estimating the abundance and size structure of an estuarine population of the sparid, *Pagrus auratus*, using a towed camera during nocturnal periods of inactivity, and comparisons with conventional sampling techniques. *Fisheries Research, 82*, 150–161. https://doi.org/10.1016/j.fishres.2006.06.024.

Pilgrim, D. A., Parry, D. M., Jones, M. B., & Kendall, M. A. (2000). ROV image scaling with laser spot patterns. *Underwater Technology, 24*, 93–103.

Pinheiro, J., & Bates, D. (2000). *Mixed-effects models in S and S-PLUS*. New York: Springer-Verlag 528 p.

Priede, I. G., Bagley, P. M., Smith, A., Creasey, S., & Merrett, N. R. (1994). Scavenging deep demersal fishes of the porcupine Seabight, north-East Atlantic: Observations by baited camera, trap and trawls. *Journal of the Marine Biological Association of the United Kingdom, 74*, 481–498. https://doi.org/10.1017/S0025315400047615.

R Development Core Team. (2015). *R: A language and environment for statistical Computing*. Vienna: R Foundation for Statistical Computing Available from: http://www.R-project.org/. March 2018.

Raymond, E., Brodeur, M., Abeels, H., & Greene, J. (2008). Bottom habitat mapping using towed underwater videography: Subtidal oyster reefs as an example application. *Journal of Coastal Research, 24*, 103–109. https://doi.org/10.2112/06-0672.1.

Rochet, M. J., Cadiou, J. F., & Trenkel, V. M. (2006). Precision and accuracy of fish length measurements obtained with two visual underwater methods. *Fishery Bulletin, 104*, 1–9.

Rohner, C., Richardson, A., Marshall, A., & Weeks, S. (2011). How large is the world's largest fish? Measuring whale sharks *Rhincodon typus* with laser photogrammetry. *Journal of Fish Biology, 78*, 378–385. https://doi.org/10.1111/j.1095-8649.2010.02861.

Rohner, C. A., Richardson, A. J., Prebble, C. E., Marshall, A. D., Bennett, M. B., Weeks, S. J., Cliff, G., Wintner, S. P., & Pierce, S. (2015). Laser photogrammetry improves size and demographic estimates for whale sharks. *PeerJ, 3*, e886. https://doi.org/10.7717/peerj.886.

Rooper, C. N. (2008). Underwater video sleds: versatile and cost effective tools for habitat mapping. In J. R. Reynolds & H. G. Greene (Eds.), *Marine habitat mapping technology for Alaska* (pp. 99–107). Alaska: Alaska Sea Grant College Program, University of Alaska Fairbanks.

Rooper, C. N., & Zimmermann, M. (2007). A bottom-up methodology for integrating underwater video and acoustic mapping for seafloor substrate classification. *Continental Shelf Research, 27*, 947–957. https://doi.org/10.1016/j.csr.2006.12.006.

Rosenkranz, G., Gallager, M., Shepard, R., & Blakeslee, M. (2008). Development of a high-speed, megapixel benthic imaging system for coastal fisheries research in Alaska. *Fisheries Research, 92*, 340–344. https://doi.org/10.1016/j.fishres.2008.03.014.

Roux, A. M., Fernandez, M., & Bremec, C. S. (1995). Preliminary survey of the benthic communities of the Patagonian shrimp fishing grounds in san Jorge gulf, Argentina. *Ciencias Marinas, 21*, 295–310.

Samoilys, M. A., & Carlos, G. (2000). Determining methods of underwater visual census for estimating the abundance of coral reef fishes. *Environmental Biology of Fishes, 57*, 289–304.

Schories, D., & Niedzwiedz, G. (2012). Precision, accuracy, and application of diver-towed underwater GPS receivers. *Environmental Monitoring and Assessment, 184*, 2359–2372. https://doi.org/10.1007/s10661-011-2122-7.

Shortis, M., Seager, J., Williams, A., Barker, B., & Sherlock, M. (2008). Using stereo-video for deep water benthic habitat surveys. *Marine Technology Society Journal, 42*, 28–37. https://doi.org/10.4031/002533208787157624.

Shortis, M., Harvey, E., & Abdo, D. (2009). A review of underwater stereo-image measurement for marine biology and ecology applications. *Oceanography and Marine Biology – An Annual Review, 47*, 257292. https://doi.org/10.1201/9781420094220.ch6.

Spencer, M., Stoner, W., Ryer, C., & Munk, J. (2005). A towed camera sled for estimating abundance of juvenile flatfishes and habitat characteristics: Comparison with beam trawls and divers. *Estuarine, Coastal and Shelf Science, 64*, 497–503. https://doi.org/10.1016/j.ecss.2005.03.012.

Stobart, B., García-Charton, J. A., Espejo, C., Rochel, E., Goñi, R., Reñones, O., Herrero, A., Crec'hriou, R., Polti, S., Marcos, C., Planes, S., & Pérez-Ruzafa, A. (2007). A baited underwater video technique to assess shallow-water Mediterranean fish assemblages: methodological evaluation. *Journal of Experimental Marine Biology and Ecology, 345*, 158–174. https://doi.org/10.1016/j.jembe.2007.02.009.

Tran, M. (2013). Mapping and predicting benthic habitats in estuaries using towed underwater video. Master thesis, University of Technology, Sydney, Australia, 170 p.

Trobbiani, G. A., &. Irigoyen, A. J. (2016). "Pepe": A novel low cost drifting video system for underwater survey. In *Proceedings of the 3rd IEEE/OES South American International Symposium on Oceanic Engineering (SAISOE)* (pp. 71–74). Buenos Aires: ARG. https://doi.org/10.1109/SAISOE.2016.7922472.

Trobbiani, G. A., & Venerus, L. A. (2015). A novel method to obtain accurate length estimates of carnivorous reef fishes from a single video camera. *Neotropical Ichthyology, 13*, 93–102. https://doi.org/10.1590/1982-0224-20140101.

Van Rooij, J. M., & Videler, J. J. (1996). A simple field method for stereo-photographic length measurement of free-swimming fish: Merits and constraints. *Journal of Experimental Marine Biology and Ecology, 195*, 237–249. https://doi.org/10.1016/0022-0981(95)00122-0.

Watson, D. L., Harvey, E. S., Anderson, M. J., & Kendrick, G. A. (2005). A comparison of temperate reef fish assemblages recorded by three underwater stereo-video techniques. *Marine Biology, 148*, 415–425. https://doi.org/10.1007/s00227-005-0090-6.

Whitmarsh, S. K., Fairweather, P. G., & Huveneers, C. (2017). What is big BRUVver up to? Methods and uses of baited underwater video. *Review in Fish Biology and Fisheries, 27*, 53–73. https://doi.org/10.1007/s11160-016-9450-1.

Willis, T. J., & Babcock, R. C. (2000). A baited underwater video system for the determination of relative density of carnivorous reef fish. *Marine and Freshwater Research, 51*, 755–763. https://doi.org/10.1071/MF00010.

Wilson, K. L., Allen, M. S., Ahrens, R. N. M., & Netherland, M. D. (2015). Use of underwater video to assess freshwater fish populations in dense submersed aquatic vegetation. *Marine and Freshwater Research, 66*, 10–22. https://doi.org/10.1071/MF13230.

Yoshihara, K. (1997). A fish body length measuring method using an underwater video camera in combination with laser discharge equipment. *Fisheries Science, 63*, 676–680. https://doi.org/10.2331/fishsci.63.676.

Zuur, A. F., Ieno, E. N., Walker, N. J., Saveliev, A. A., & Smith, G. M. (2009). *Mixed effects models and extensions in ecology with R*. New York: Springer 608 p.